Title

Interplay of matrix stiffness and protein tethering in stem cell differentiation

Authors

Wen, JH
Vincent, LG
Fuhrmann, A
et al.

Publication Date

2014-08-10

DOI

10.1038/nmat4051

Peer reviewed

nature materials

ARTICLES

PUBLISHED ONLINE: 10 AUGUST 2014 | DOI: 10.1038/NMAT4051

Interplay of matrix stiffness and protein tethering in stem cell differentiation

Jessica H. Wen[1†], Ludovic G. Vincent[1†], Alexander Fuhrmann[1], Yu Suk Choi[1‡], Kolin C. Hribar[2], Hermes Taylor-Weiner[1], Shaochen Chen[2] and Adam J. Engler[1,3*]

Stem cells regulate their fate by binding to, and contracting against, the extracellular matrix. Recently, it has been proposed that in addition to matrix stiffness and ligand type, the degree of coupling of fibrous protein to the surface of the underlying substrate, that is, tethering and matrix porosity, also regulates stem cell differentiation. By modulating substrate porosity without altering stiffness in polyacrylamide gels, we show that varying substrate porosity did not significantly change protein tethering, substrate deformations, or the osteogenic and adipogenic differentiation of human adipose-derived stromal cells and marrow-derived mesenchymal stromal cells. Varying protein–substrate linker density up to 50-fold changed tethering, but did not affect osteogenesis, adipogenesis, surface–protein unfolding or underlying substrate deformations. Differentiation was also unaffected by the absence of protein tethering. Our findings imply that the stiffness of planar matrices regulates stem cell differentiation independently of protein tethering and porosity.

The stiffness of the extracellular matrix (ECM) has been shown to regulate both short- and longer-term cell functions such as cell spreading[1] and stem- and progenitor- cell phenotype changes on planar substrates[2–7]. For example, many types of adult stromal cell grown on substrates of stiffness similar to that of the osteoid or muscle express lineage markers of terminally differentiated cells found in those tissues[3,4,6]. Common myosin-based contractile mechanisms are needed for matrix-induced differentiation in two dimensions[3,8–10]. However, in three dimensions, a labile[11] or degradable matrix[12], which permits cells to first spread and then adhere to the ECM, is required. Similarly, force-mediated protein unfolding in the ECM *in vivo* regulates cell responses as a function of stiffness[13,14]. Whereas creating three-dimensional matrices has become a widespread approach towards understanding how the matrix affects cell fate, the regulatory role of substrate-anchored fibrous- protein deformations on stem cell fate in two dimensions is still unclear.

Recent literature suggests that the mechanical resistance provided by the ECM, which opposes myosin-based contractility that results in cell signalling and differentiation, could, for planar cultures, arise from protein tethers rather than substrate stiffness[15]. As most synthetic planar matrices are not normally cell- adhesive, an adhesive layer of matrix protein is attached to the hydrogel surface and covalently 'tethered' to the substrate surface at distinct anchoring points. Thus, changing protein–substrate linker density or substrate porosity can vary the length of the fibre segment between two adjacent anchoring points. When a load is applied perpendicularly to the fibre segment, its deflection is directly related to the load applied, fibre stiffness, and the cube of the length of the fibre segment[15,16]. If enough resistance were present in these tethers, stem cells could differentiate independently of substrate stiffness. However, it is unclear what the length of these tethers is and how it compares to substrate deformations[17], which have been implicated in mechanotransduction and hence stem cell differentiation[18]. Thus, it is critical to decouple protein tethering and substrate stiffness to determine whether and how these factors collectively regulate stem cell differentiation.

Tuning hydrogel porosity independently of stiffness

Tuning the ratio of acrylamide monomer and bis-acrylamide crosslinker can change the porosity of the polyacrylamide (PA) hydrogel, that is, the distance between tethering points, while maintaining constant stiffness. To accomplish this, three separate acrylamide/bis-acrylamide formulations were polymerized to yield hydrogels of ~4, ~13 and ~30 kPa (Fig. 1a), which correspond to the stiffness of adipose tissue, muscle and osteoid[2,3,6,19–21], respectively. Differences in volume and mass swelling ratios between each of the hydrogels with similar stiffness suggest significant differences in porosity among each substrate subgroup (Supplementary Fig. 1a,b). The radius of gyration of extended DNA may be used to estimate the effective maximum pore size of the hydrogel[22]. DNA size standards were exposed to an electrophoretic gradient in swollen and unconfined 4 and 30 kPa PA hydrogels to further quantify hydrated pore size. For 30 kPa hydrogels, a 45 nm DNA fragment failed to migrate through the 8/0.55 formulation, indicating that the maximum pore size of this formulation is between 23 and 45 nm. Larger DNA fragments migrated through the 10/0.3 and 20/0.15 gel formulations, indicating that the approximate pore sizes are between 88 and 166 nm for both formulations; differences in DNA mobility suggest that the two gels have pore sizes that differ within this range. Similarly, differences in DNA mobility suggest that the three 4 kPa formulations yield hydrogels with different pore sizes (Supplementary Fig. 1c). Scanning electron microscopy (SEM) of dried PA hydrogels showed increasing pore sizes with increasing acrylamide and decreasing bis-acrylamide concentrations for the 4, 13 and 30 kPa hydrogel formulations (Fig. 1b); these data are consistent with pore size trends in hydrated measurements and together demonstrate that

[1]Department of Bioengineering, University of California, San Diego, La Jolla, California 92093, USA, [2]Department of Nanoengineering, University of California, San Diego, La Jolla, California 92093, USA, [3]Sanford Consortium for Regenerative Medicine, La Jolla, California 92037, USA. †These authors contributed equally to this work. ‡Present address: Kolling Institute of Medical Research, Royal North Shore Hospital, The University of Sydney, Sydney, New South Wales 2065, Australia. *e-mail: aengler@ucsd.edu

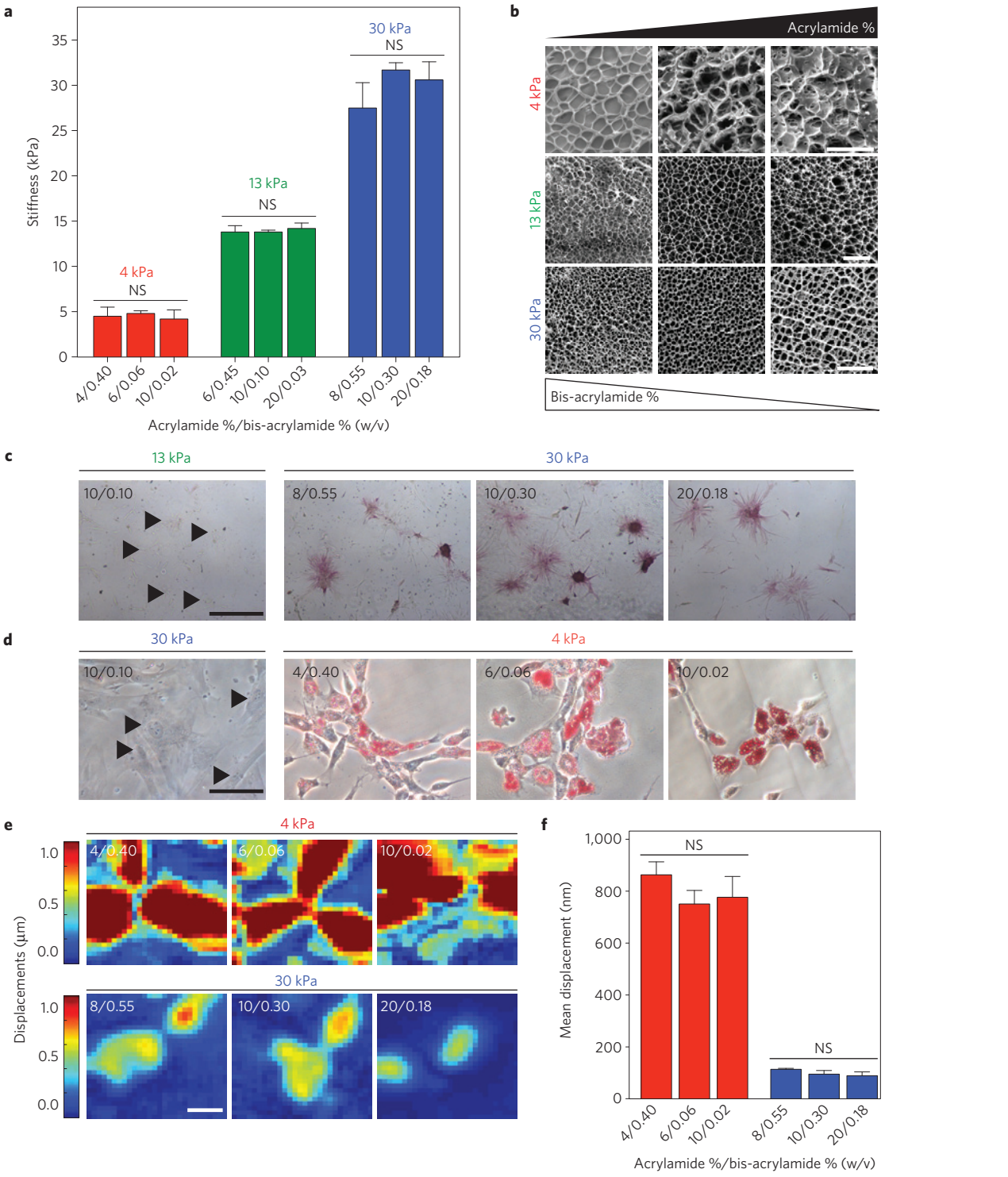

Figure 1 | Influence of substrate porosity on ASC differentiation. a, Elastic modulus measured by AFM ($n=3$) for the indicated acrylamide/bis-acrylamide ratios (mean ± s.d.). **b**, SEM images of PA hydrogels made with varying monomer-to-crosslinker ratios as indicated. Scale bars, 50 μm (top and bottom), 10 μm (middle). **c**, ALP staining of ASCs on 13 and 30 kPa hydrogels of the indicated compositions after 14 days of culture in normal media. Arrowheads indicate stained but yet negative cells. Scale bar, 500 μm. **d**, ORO staining of ASCs on 4 kPa and 30 kPa hydrogels of the indicated compositions after 7 days of culture in adipogenic induction media. Arrowheads indicate stained but yet negative cells. Scale bar, 100 μm. **e**, Displacement maps of embedded fluorescent particles resulting from ASC traction forces on 4 kPa and 30 kPa hydrogels of the indicated compositions. Scale bar, 50 μm. **f**, Quantification of mean displacement was plotted for hydrogels of the indicated composition and stiffness range ($n>20$; mean ± s.e.m.; NS, not significant).

increasing the concentration of the bis-acrylamide crosslinker decreases the relative pore size without substantially changing the modulus of the hydrogel. However, it is important to note here that pore sizes derived from SEM images of freeze-dried hydrogels are probably not representative of actual substrate pore sizes in a hydrated state. Cells interact with hydrated substrates *in vitro*, and thus SEM images are provided only for relative comparison of pore sizes for the hydrogel formulations reported.

Differentiation does not depend on porosity

Human adipose stromal cells (ASCs) were plated onto 13 and 30 kPa PA hydrogels from the formulations indicated in Fig. 1c. After 14 days of culture in normal growth media, osteogenic differentiation (as indicated by positive alkaline phosphatase (ALP) staining in subconfluent cells) occurred regardless of hydrogel formulation and was directly dependent on substrate stiffness, as 13 kPa substrates were negative for ALP (Fig. 1c). Further confirmation of this is demonstrated by positive and nuclear localized RUNX2 immunofluorescence staining after 7 days in culture on all 30 kPa hydrogels (Supplementary Fig. 2a). The expression levels of the early osteogenic markers ALP and RUNX2 suggest that changes in porosity independently of stiffness have no noticeable effects on differentiation for the range of hydrogel formulations tested. However, allowing cells to reach confluence in normal media on any hydrogel formulation was sufficient to override substrate- stiffness-mediated differentiation and induce osteogenesis as previously observed[15], most likely owing to other factors including cell–cell signalling and secreted paracrine factors (Supplementary Fig. 3). To avoid complications arising from confluent monolayers and to focus only on cell–ECM signalling, osteogenic- differentiation studies were conducted at low cell densities. Mesenchymal stromal cells (MSCs), another commonly used cell type in differentiation experiments, also stained positive for ALP after 14 days in culture on the three 30 kPa hydrogel formulations (Supplementary Fig. 3b), implying that substrate porosity has little effect on multiple stem cell types. In addition, after 14 days in culture in adipogenic induction media, adipogenic differentiation, as assessed by oil red O (ORO) presence, was found in over 40% of ASCs on all 4 kPa substrates regardless of hydrogel formulation and was directly dependent on substrate stiffness, as 30 kPa substrates were negative for ORO (Fig. 1d and Supplementary Fig. 2c).

As cell–ECM signalling depends on contractility, and differences in contractility have been shown to regulate differentiation[3,8–10], displacement maps of embedded fluorescent particles resulting from ASC traction forces on all 4 and 30 kPa hydrogel formulations were computed (Fig. 1e and Supplementary Fig. 4) using traction force microscopy[23] (TFM). Mean displacements were similar between all formulations of 4 and 30 kPa hydrogels, but different between hydrogels of different stiffness (Fig. 1f). These data indicate that over the range of formulations tested, hydrogel deformations due to cell contractions are similar regardless of porosity but are dependent on stiffness (Fig. 1e,f). Taken together, these data show that varying porosity alone does not seem to be sufficient to alter the fate of two different adult stem cell sources.

Modulating protein tethering by changing linker density

Culturing cells on synthetic hydrogels requires the covalent coupling of a cell-adhesive matrix protein, such as collagen type I, to the hydrogel surface using a protein–substrate linker, such as sulpho-SANPAH (ref. 1). Changing the concentration of this linker has been proposed to modulate protein tethering[15]. To modulate the tethering of fibrous collagen to PA hydrogels, we tuned the surface density of anchoring points by varying the concentration of sulpho-SANPAH, thus varying the average distance between adjacent anchoring points. To assess possible differences in the physical structure or total amount of bound protein, immunofluorescence staining of collagen covalently coupled to PA substrates activated with varying concentrations of sulpho-SANPAH was performed. Images revealed noticeable surface heterogeneity, making quantification of absolute protein amount difficult (Supplementary Fig. 5a); this was further illustrated by collagen pixel intensity histograms for 13 and 30 kPa hydrogels over a range of sulpho-SANPAH concentrations (Supplementary Fig. 5b). Fluorescent detection was unable to quantify surface-bound protein as previously suggested[15]. To directly quantify collagen tethering, we obtained individual force spectrograms (Supplementary Fig. 6a) from microindentations of collagen-coated PA hydrogels. Substrates activated with a range of sulpho-SANPAH concentrations were indented using a probe functionalized with an anti-collagen type I antibody (Fig. 2a). As the tip retracts from the surface, the collagen unfolds and/or stretches until the antibody–protein bonds rupture (Supplementary Fig. 6a). Force spectrograms were analysed to locate rupture events and to determine the force at rupture, that is, the force required to break a protein–antibody bond, and the rupture length that is, the deflection of the collagen fibre segment at rupture. Larger rupture forces and a greater number of rupture events were detected in the presence of collagen I (Fig. 2b, left and Supplementary Fig. 6b) and indicate that the antibody was specifically binding and loading collagen. Decreasing rupture length with increasing sulpho-SANPAH concentration (Fig. 2b, right) confirmed that the number of protein anchoring points scaled with sulpho-SANPAH concentration without substantial changes in rupture force (Fig. 2b). This trend held for all 30 kPa formulations tested despite significant changes in the number of available protein anchoring sites, which is proportional to acrylamide concentration. We observed differences in rupture length between sulpho-SANPAH concentrations across hydrogel formulations (Fig. 2c, grey versus white bars), indicating that anchoring sites must not be saturated. Furthermore, for a given sulpho-SANPAH concentration, although small differences in average rupture length were detected between the three 30 kPa hydrogel formulations, that is, <40 nm, these differences were smaller than the changes in pore size, which were up to 120 nm (Supplementary Fig. 1c). Thus, differences in rupture lengths between the hydrogel formulations are not likely to be due to porosity changes.

Differentiation does not depend on tethering

To investigate whether or not tethering impacts stem cell fate, subconfluent ASCs and MSCs were cultured in normal growth medium on 30 kPa hydrogels over a range of sulpho-SANPAH concentrations and assessed for osteogenic differentiation. Positive ALP and RUNX2 staining was observed on all 30 kPa hydrogels regardless of sulpho-SANPAH concentration, hydrogel formulation and cell type (Fig. 2d and Supplementary Fig. 7). ASCs were also cultured on 4 kPa hydrogels over a range of sulpho-SANPAH concentrations, and ORO expression was observed in over 30% of ASCs regardless of sulpho-SANPAH concentration (Supplementary Fig. 8). Together, these data indicate that the degree of collagen tethering to the substrate surface had no observable effect on stem cell fate, unlike what has been suggested[15]. Myosin contractility deforms the ECM and is required for matrix-induced differentiation[3,8–10]; thus, to confirm differentiation results, substrate displacements for hydrogels across a range of sulpho-SANPAH concentrations were mapped using TFM (Fig. 2e). Average displacements of beads embedded in hydrogels were independent of sulpho-SANPAH concentration and dependent only on substrate modulus (Fig. 2f), suggesting that for the range of protein–substrate linker concentrations used in this study, the surface density of collagen fibre covalent anchoring points has no impact on how cells deform the underlying substrate.

To determine whether or not differences in rupture lengths, that is, tethering, detected by force spectrograms could be felt by cells on a molecular scale, a fibronectin Förster resonance energy transfer (FRET) sensor[14] was covalently attached to hydrogels in place of collagen. Cell-generated forces unfold the protein thus increasing the distance between paired fluorescent probes, which results in a decrease in the FRET ratio (Supplementary Fig. 9a) that can also be shown by chemical denaturation (Supplementary Fig. 9b,c). Changing sulpho-SANPAH concentration has no statistical effect on the FRET ratio of fibronectin underneath spread ASCs regardless

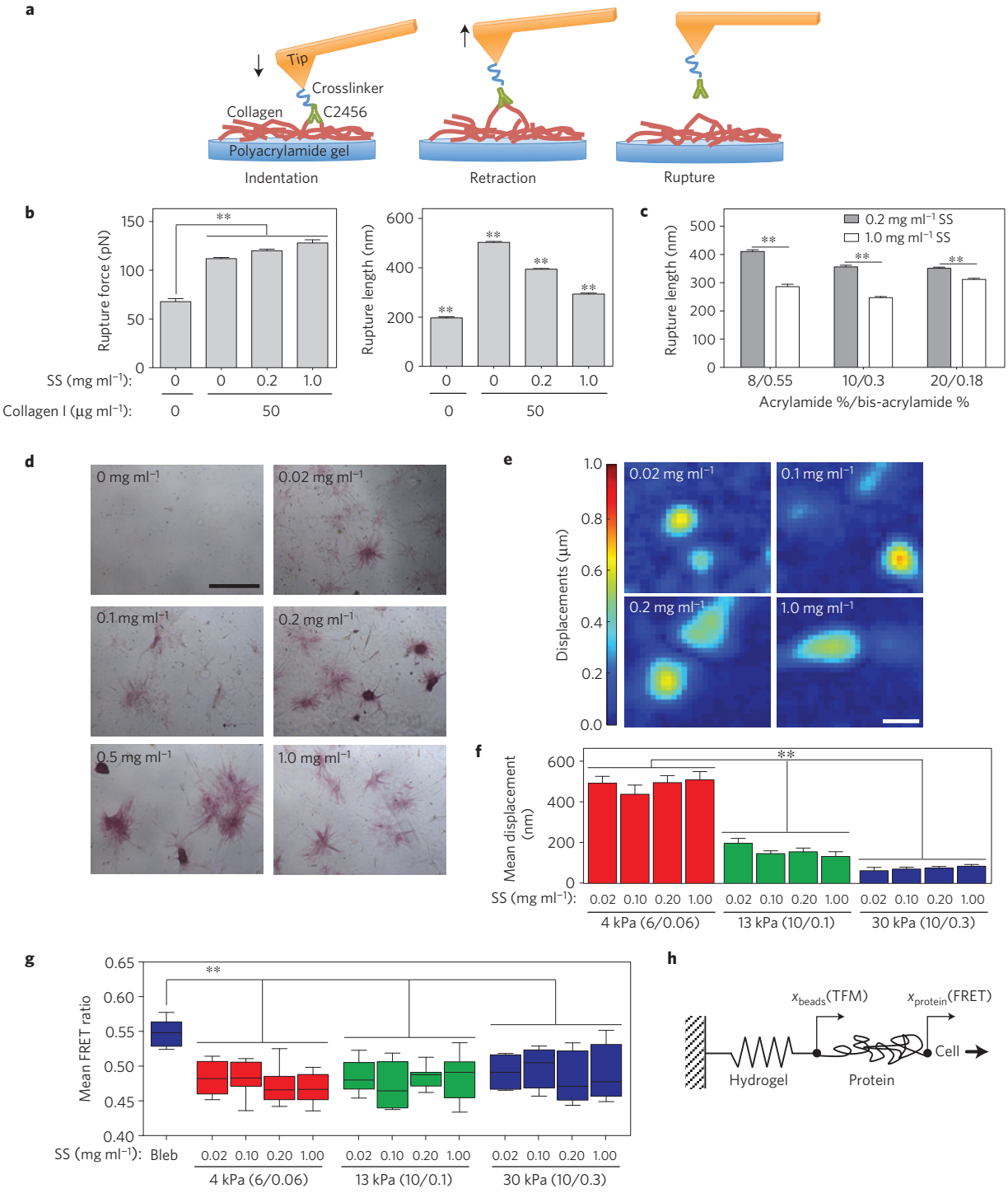

Figure 2 | Influence of protein tethering on ASC differentiation. a, Schematic depicting the interaction between an AFM tip (orange) functionalized with a collagen I antibody (C2456; green) and the hydrogel (blue) functionalized with bound collagen I (red). The black arrow indicates the direction of motion. A rupture event occurs following retraction of the tip from the surface. **b**, Measured rupture force (left) and rupture length (right) for rupture events that occurred on 10/0.3 30 kPa hydrogels activated with the indicated sulpho-SANPAH (SS) and collagen I concentrations ($n=500$; mean ± s.e.m.; $^{**}P<0.0001$). **c**, Rupture length was measured for rupture events that occurred on 30 kPa hydrogels with the indicated monomer-to-crosslinker ratios. Hydrogels were activated with either 0.2 mg ml^{-1} or 1 mg ml^{-1} sulpho-SANPAH. ($n=500$; mean ± s.e.m.; $^{**}P<0.0001$). **d**, Images of ASCs stained for ALP expression on 10/0.3 hydrogels as a function of sulpho-SANPAH concentration after 14 days of culture in normal media. Scale bar, 500 μm. **e**, Displacement maps of embedded fluorescent particles resulting from ASC traction forces on 10/0.3 hydrogels for a range of indicated sulpho-SANPAH concentrations. Scale bar, 50 μm. **f**, Quantification of mean bead displacement for the indicated hydrogel stiffness and composition as well as sulpho-SANPAH (SS) concentration ($n=20$; mean ± s.e.m.; $^{**}P<0.0001$). **g**, Measured fibronectin FRET intensity ratio for ASCs on 4, 14 and 30 kPa hydrogels activated with the indicated concentrations of sulpho-SANPAH ($n=8$; $^{**}P<0.001$). **h**, Proposed model of a cell on a protein-coated substrate attached to a rigid base (glass coverslip) where cell forces are translated through the protein and through the substrate. Deformations of the substrate are measured by TFM and deformations of the protein are measured by FRET.

of hydrogel formulation, whereas perturbing myosin contractility using blebbistatin caused a significant increase in the FRET ratio (Fig. 2g and Supplementary Fig. 9d). Thus, molecular conformational changes in protein caused by ASC traction forces are similar regardless of protein–substrate linker concentration, implying that ASCs deform the surface protein similarly on all sulpho-SANPAH activated hydrogels. On the basis of these findings, we propose that cells deform both the adhesive protein on the hydrogel surface as well as the underlying PA substrate according to the model depicted in Fig. 2h. Cell forces are translated sequentially through the protein layer and the hydrogel. However, our findings suggest that the degree of coupling of the protein to the substrate does not influence substrate deformation and thus differentiation; therefore, it was not depicted in Fig. 2h.

Differentiation occurs in the absence of tethering

To demonstrate that stiffness-induced differentiation is possible in the absence of fibrous protein tethering, RGD, a short cell-adhesive peptide from fibronectin[24], was directly incorporated into the PA backbone by including acrylated polyethylene glycol bound to RGD (acrylated-PEG–RGD) during polymerization rather than by tethering an adhesive protein to the substrate. Three separate hydrogel formulations with 0.1, 0.5 and 2.5 mM RGD yielding the same gel stiffness were made for 4, 13 and 30 kPa substrates using the acrylamide/bis-acrylamide ratios listed above (Fig. 3a). A hydroxycoumarin dye-conjugated acrylated-PEG–RGD confirmed that the peptide was incorporated in a dose-dependent manner (Fig. 3b). SEM images of dried hydrogels show similar pore sizes regardless of the concentration of acrylated-PEG–RGD incorporated within each substrate (Fig. 3c). This ensures that differentiation effects can be attributed to changes in adhesive-peptide density and not porosity. Furthermore, to ensure that the PEG moiety does not act as a tether, individual force spectrograms were obtained from biotin-terminated PEG-coated PA hydrogels and an avidin-functionalized probe. Larger rupture forces and a greater number of rupture events were detected on substrates before blocking with excess avidin in solution (Fig. 3d, left and middle), which indicate that the avidin-functionalized probe was specifically bound to the biotin-coated surface. Rupture lengths before and after blocking were not statistically different (Fig. 3d, right) and were similar to rupture lengths measured on control PA substrates with no surface coating (Fig. 2b, right). In contrast to collagen-coated PA substrates that exhibited significantly greater rupture lengths, the deformations of the PEG moiety are minimal. Thus, PA–PEG–RGD substrates are a valid culture platform absent of protein tethering for the given concentration range and size of PEG tested. ASCs were then cultured for 14 days in normal growth media to determine whether differentiation was possible without tethering over the range of peptide concentrations tested. ASCs underwent osteogenic differentiation on 10/0.3 30 kPa hydrogels independently of RGD concentration (Fig. 3e). Furthermore, osteogenic differentiation was seen in ASCs and MSCs cultured on all 30 kPa hydrogel formulations with 2.5 mM RGD (Fig. 3f and Supplementary Fig. 10). Together, these data suggest that differentiation occurs in the absence of fibrous protein tethering over the range of peptide concentrations tested. Cell-generated substrate displacements were similar to that of collagen-coated hydrogels (Fig. 3g), lending further evidence that matrix-induced differentiation operates through common myosin-based contractile mechanisms given that differentiated cells on these and collagen-coated hydrogels were similar.

Cell spread area on PA and PDMS substrates

To further support the claim that stiffness mediates cell functions generally, we observed the basic behaviour of cell spreading on PA–PEG–RGD hydrogels in the absence of protein tethers. ASC spread area 24 h after seeding scaled with increasing hydrogel stiffness (Supplementary Fig. 11a). This suggests that stiffness is an important physical factor regardless of how adhesive ligands are presented (although dependent on concentration[25]). To determine whether or not this phenomenon is specific to acrylamide-based systems, polydimethylsiloxane (PDMS) substrates were fabricated with base-to-curing ratios of 100:1, 75:1 and 50:1 to modulate stiffness as noted previously[15]. These substrates were not functionalized with adhesive protein. Without covalently attaching or tethering ligands to the surface, cell adhesion and spreading was still possible for all substrates, owing to the well-known fouling properties of PDMS. Furthermore, cell spread area was similar on all substrates (Supplementary Fig. 11b). This observation is in agreement with previous observations that imply stiffness-independent cell spreading on PDMS substrates[15], suggesting that cells may sense similar mechanical cues on the three PDMS formulations.

PDMS mechanical properties on a cell-sensing scale

Owing to a lack of correlation between cell spread area and PDMS base-to-curing ratio, we independently measured PDMS stiffness by atomic force microscopy (AFM) microindentation. The stiffnesses of 50:1 and 100:1 PDMS were found to be 250 and 550 kPa (Supplementary Fig. 12a)—orders of magnitude greater than previously reported[15]. As PDMS has previously been shown to be viscoelastic at higher base-to-curing ratios[26], substrates were instead indented using different indenter geometries and at different indentation speeds. Indenting substrates with two different probes and a wide range of indentation speeds confirmed the viscoelastic behaviour of PDMS (Supplementary Fig. 12b) and suggests that different methods of characterization may account for discrepancies in reported values of PDMS stiffness.

Given the lack of consensus on measuring the mechanical properties of PDMS, it is important to use the most appropriate technique to closely mimic cell–substrate interactions. Cells pull against substrates at 20–120 nm s^{-1}, resulting in deformations that scale inversely with stiffness[17,27] (Fig. 4a). We can match AFM tip- retraction velocity to the pulling velocity and size of focal adhesions. Consequently, we can simulate these dynamically fluctuating pulling events by analysing the retraction curves (as opposed to indentation curves) obtained by AFM where the tip has pulled and deformed the material above the surface (Fig. 4b). The substrate stiffness is determined by fitting the linear region beginning at the contact point with the (undeformed) surface ($F = 0$ pN) to where the force reaches -100 pN (Fig. 4c). PA hydrogels of 1 and 30 kPa demonstrated little variation in stiffness over a range of cell-relevant strains[26] and retraction speeds[17,27]. The stiffnesses of 50:1 and 100:1 PDMS were both significantly higher than the PA hydrogels, and the stiffness of 100:1 PDMS increases 50-fold over the range of retraction velocities tested (Fig. 4d). These data confirm that 100:1 PDMS is highly viscoelastic and 50:1 PDMS is predominantly elastic, but both are stiff over cell-relevant strains in agreement with previous data[26]. Although previous studies have noted lower stiffness values of PDMS for the same cure ratios[15], it is well known that the mechanical properties of PDMS are different at the cellular mechanosensing scale than at the macroscopic scale[28]. At the scale at which a cell mechanosenses[17,27], both 50:1 and 100:1 PDMS substrates are stiffer than 30 kPa PA hydrogels (Fig. 4d). This provides a reasonable explanation as to why cell spreading (Supplementary Fig. 11b) and osteogenic differentiation (Fig. 4e), neither of which changed with cure ratio, were previously reported to be stiffness independent[15]. We note here, however, that it is possible to decrease the effective stiffness of PDMS by fabricating microposts of identical cure ratios but different heights. In ref. 28, it was found that MSC contractility and differentiation towards adipogenic or osteogenic lineages scaled as a function of effective stiffness pillar height. Thus, even

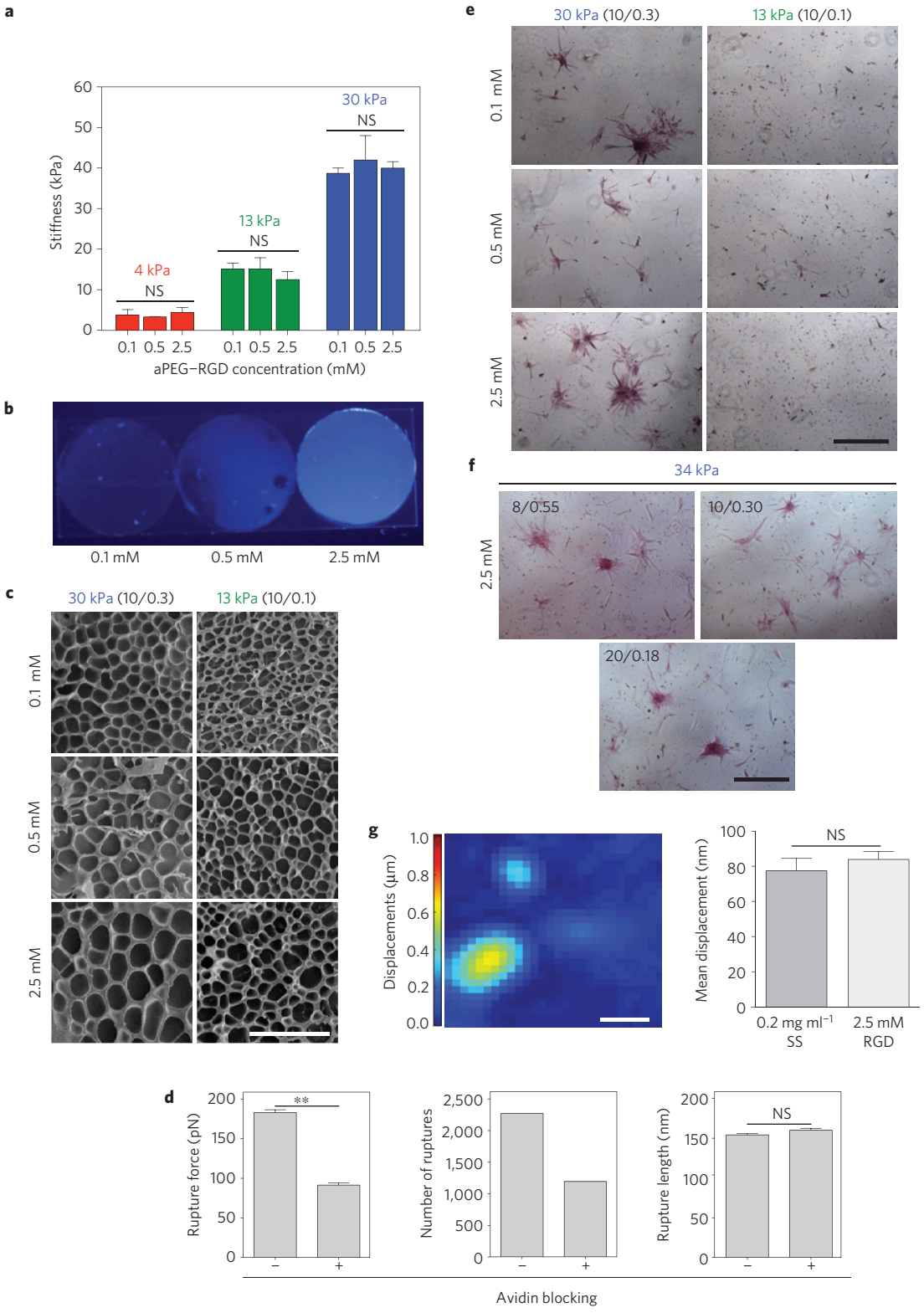

Figure 3 | Direct incorporation of a short adhesive peptide to the PA substrate. a, Elastic modulus measured by AFM (mean ± s.d.; $n=3$; NS, not significant). **b**, aPEG–RGD–dye incorporation is detected under ultraviolet light. **c**, SEM images of PA hydrogels of the indicated stiffness made with varying RGD concentration. Scale bar, 50 μm. **d**, Measured rupture force (left), number of events (middle), and rupture length (right) for rupture events that occurred on 10/0.3 30 kPa hydrogels coated with PEG–biotin ($n=1,000$; mean ± s.e.m.; NS, not significant; $^{**}P<0.0001$). **e**, ALP staining of ASCs on 13 kPa and 30 kPa hydrogels with low, medium and high concentrations of RGD. Scale bar, 500 μm. **f**, ALP staining of ASCs on 30 kPa hydrogels of varying monomer-to-crosslinker ratio and constant high concentration of RGD after 14 days of culture in normal media. Scale bar, 500 μm. **g**, Representative displacement map (left) of embedded fluorescent particles resulting from ASC traction forces on a 30 kPa hydrogel with 2.5 mM RGD. Mean displacement is shown (right) for a collagen-coated hydrogel (0.2 mg ml^{-1} sulpho-SANPAH and 50 μg ml^{-1} collagen I) and a PA–PEG–RGD hydrogel (2.5 mM RGD). ($n=30$; mean ± s.e.m.; NS, not significant; scale bar, 50 μm.)

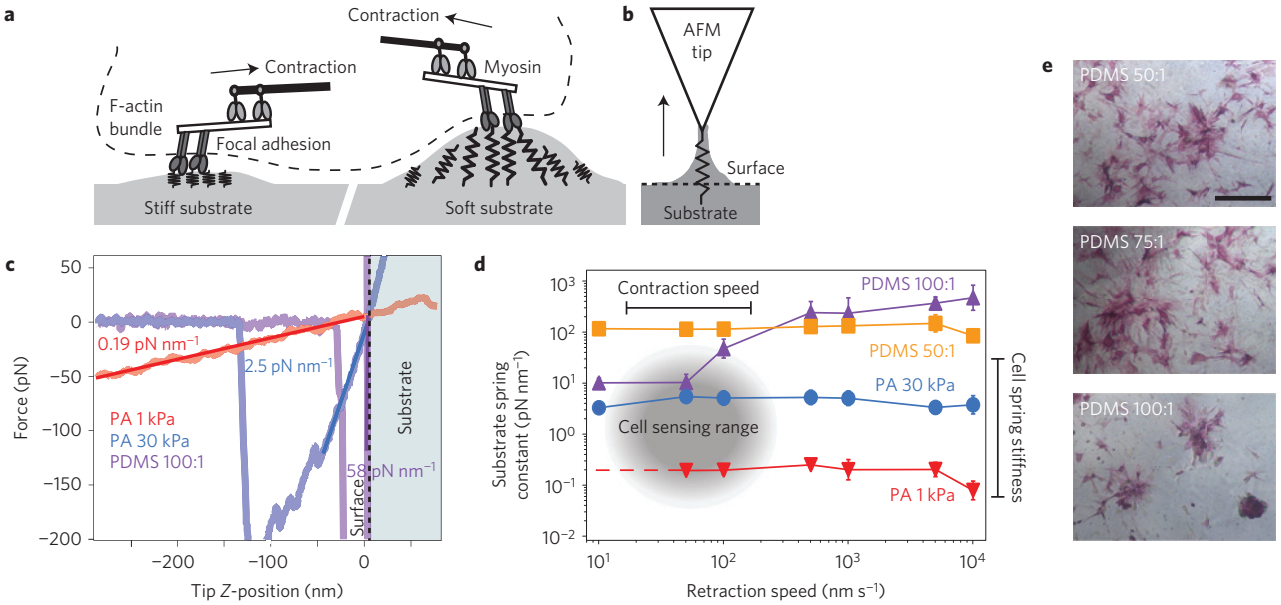

Figure 4 | Cells sense by contracting against their substrates. a, Schematic depicting how cells dynamically deform soft and stiff substrates by pulling (and not pushing) through myosin contractions. Softer substrates are deformed to a greater extent than stiffer substrates. **b**, Schematic depicting the interaction between an AFM tip and the surface of a substrate. The arrow indicates the direction of motion of the tip during retraction. **c**, Representative retraction curves for 1 and 30 kPa PA hydrogels and a 100:1 PDMS substrate. The dashed line indicates the point at which the tip is no longer indenting into the substrate (shaded light blue). Substrate stiffness is calculated by fitting the linear region of the retraction curve starting at the (undeformed) surface. **d**, Substrate spring constant determined by the method depicted in **c** for 1 and 30 kPa PA hydrogels and 50:1 and 100:1 PDMS substrates as a function of AFM tip retraction speed (mean ± s.d.). Cells are sensitive to substrate stiffnesses of 1–100 kPa. Previously measured myosin contraction speeds range from 10–100 nm s^{-1} (grey). **e**, ALP staining of ASCs on PDMS substrates after 7 days of culture in normal media. Scale bar, 500 μm.

in PDMS systems where cure ratio is not directly modulated, effectively modulating stiffness can still yield mechanically driven differentiation.

PDMS substrates do not support protein tethering

To address the possibility of fibrous protein tethering on PDMS, 50:1 PDMS substrates were examined using force spectroscopy. When 50:1 PDMS substrates were pre-incubated in a collagen solution, rupture events with lengths and forces much greater than that of PA substrates were detected (Fig. 5a), confirming that collagen nonspecifically adsorbs to PDMS. Attempting to functionalize PDMS with sulpho-SANPAH before collagen incubation[15] did not alter the rupture force (Fig. 5b). However, the rupture length markedly increased from 450 nm to 1.5 μm, which is larger than cell deformations on stiff PA substrates (Figs 2g and 5a). This observation is opposite to what was seen with PA; treating PA with sulpho-SANPAH increases fibrous- collagen tethering to PA, consequently decreasing the rupture length (Fig. 2b).

The increased rupture lengths seen in PDMS may be attributed to the formation of long chains of collagen forming on the PDMS surface as collagen contains many primary amines for sulpho-SANPAH to crosslink, whereas PDMS is void of amines (Supplementary Fig. 13a, left). In this hypothesis, sulpho-SANPAH is not directly coupled to the PDMS surface, but rather only to collagen chains. To test this hypothesis, substrates were functionalized with sulpho-SANPAH before incubation in NH_2–PEG–biotin, which has only one free primary amine (Supplementary Fig. 13a, right). Rupture lengths and forces obtained from force spectrograms using avidin tips were similar on biotin-coated substrates functionalized with and without sulpho-SANPAH (Fig. 5a).

To further confirm that sulpho-SANPAH does not react with PDMS, amines were covalently bound to PDMS substrate surfaces using the chemistry outlined in Supplementary Fig. 13b. At least one rupture event was detected in more than 90% of the force spectrograms obtained from biotin-coated samples. In contrast, rupture events were detected in only 30% of the force spectrograms obtained from biotin-coated but not amine-functionalized PDMS samples independently of sulpho-SANPAH (Fig. 5b). Thus, it is clear that the sulpho-succinimidyl group requires amines to form a covalent bond. Regardless of ultraviolet treatment, PDMS surfaces do not display free amines, and thus protein cannot be covalently bound to the surface through sulpho-SANPAH. Previous efforts do not seem to have amine-functionalized PDMS (ref. 15), and thus it is difficult to attribute fibrous- protein tethering on PDMS to cell spreading and differentiation. These results, in conjunction with cure ratio-independent stem cell spreading (Supplementary Fig. 11b) and differentiation (Fig. 4e), emphasize the shortcomings of PDMS as a model system to investigate stiffness-dependent behaviour over a relevant cell-sensing range[28]. Elastic two-dimensional hydrogel systems with controlled stiffness such as PA, PEG (ref. 29), hyaluronic acid[30,31] and alginate[32] are better suited to investigate these cell behaviours.

Summary

The commonly used PA hydrogel system is easily tuned to modulate substrate porosity, and in combination with different concentrations of sulpho-SANPAH, provides a platform to investigate how substrate stiffness, porosity and ligand tethering affect stem cell fate. The data presented here provide direct evidence that the mechanical feedback provided by hydrogel deformations on planar matrices regulates osteogenic and adipogenic differentiation of ASCs and MSCs independently of protein tethering and substrate porosity. Furthermore, these data indicate that substrates have fibrous-protein tethers as previously suggested[15]; however, these tethers are not essential for the osteogenic and adipogenic differentiation of ASCs and MSCs. This work further highlights the importance of bulk matrix stiffness as the main mechanical regulator of stem cell differentiation.

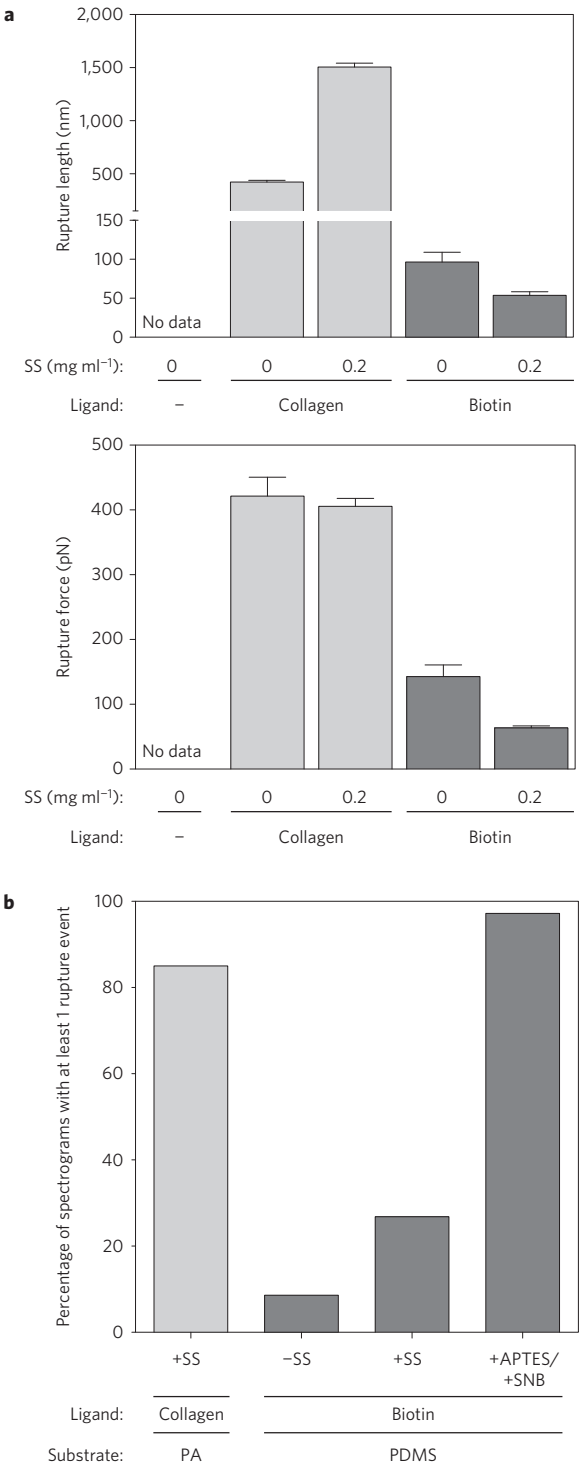

Figure 5 | Atomic force spectrography analysis of ligand-coated PDMS substrates. a, Measured rupture length (top) and rupture force (bottom) for rupture events detected on 50:1 PDMS substrates activated with the indicated sulpho-SANPAH (SS) and collagen or NH_2–PEG–biotin concentrations (mean ± s.e.m.). No data indicates that no rupture events were detected. **b**, Percentage of spectrograms with at least one rupture event on PA and PDMS substrates activated with the linkers and ligands shown.

Methods

PA gels. Glass coverslips were functionalized using 3-(trimethoxysilyl)propyl methacrylate to facilitate covalent attachment of hydrogel substrates to glass. A polymer solution containing acrylamide monomers, crosslinker *N*,*N* methylene-bis-acrylamide, ammonium persulphate and *N*,*N*,*N*′,*N*′-tetramethylethylenediamine (TEMED) was prepared. The polymerizing solution was sandwiched between a functionalized coverslip and a dichlorodimethylsilane-treated slide to ensure easy detachment of hydrogels. The ratio of acrylamide%/bis-acrylamide% was varied to control hydrogel stiffness and porosity. To allow for cell adhesion and fibrous- protein tethering, substrates were incubated in 0.02, 0.1, 0.2, 0.5 or 1 mg ml^{-1} *N*-sulphosuccinimidyl-6-(4′-azido-2′-nitrophenylamino) hexanoate (sulpho-SANPAH), activated with ultraviolet light, washed, and then incubated in collagen overnight. For AFM experiments, 0.5 mg ml^{-1} amine–PEG3400–biotin was used instead of collagen. Coated hydrogels were ultraviolet sterilized before use in cell culture.

PA–PEG–RGD gels. PA–PEG–RGD hydrogels were fabricated by incorporating 0.1 mM, 0.5 mM or 2.5 mM acrylated-PEG3400–GRGD-amide (aPEG–RGD) into the polymerizing solution described above. To visualize RGD concentration differences, a fluorescent hydroxycoumarin dye was conjugated to the peptide.

PDMS substrates. PDMS was mixed at various elastomer base/curing agent ratios (50:1, 75:1, 90:1, 100:1), thoroughly mixed, and degassed under vacuum before pouring directly into multi-well plates or onto coverslips and baked overnight. In certain instances, substrates were functionalized with sulpho-SANPAH and ligand (Supplementary Information and Supplementary Fig. 13a). For covalent attachment of moieties to the surface, PDMS substrates were treated with ultraviolet/ozone following an incubation under vacuum in the presence of (3-aminopropyl)triethoxysilane. Surfaces were then incubated in sulpho-NHS–biotin (Supplementary Fig. 13b).

SEM. PA and PA–PEG–RGD solutions were polymerized. Hydrogels were swelled in water overnight, flash frozen, then lyophilized overnight. Lyophilized samples were sputter coated with iridium.

DNA gel electrophoresis. DNA ladders were run through PA electrophoresis gels in TAE buffer with ethidium bromide at 30 V for 14 h. DNA fragment lengths were converted to radius of gyration as described elsewhere[22].

Stem cell culture. Human ASCs were isolated from freshly aspirated human subcutaneous adipose tissue according to the method described elsewhere[33]. Commercially available MSCs were purchased. MSCs and ASCs were cultured in Dulbecco's modified eagle medium with fetal bovine serum and antibiotics. For differentiation experiments, MSCs and ASCs were seeded on PA and PDMS substrates at a density of 1,000 cells cm^{-2} and on PA–PEG–RGD gels at a density of 2,000 cells cm^{-2}. See Supplementary Information for inductive media formulations.

Immunofluorescence. Cells were fixed, permeabilized and then stained with rhodamine phalloidin and Hoechst. For osteogenic differentiation studies, cells were stained with RUNX2. To quantify RUNX2 expression, CellProfiler[34] (Broad Institute) was used to measure cytoplasmic and nuclear fluorescent intensities using the nuclei and cell outlines as masks to define these regions of interest in the RUNX2 fluorescent channel.

Differentiation assays. ASCs and MSCs were stained for ALP and ORO as per manufacturer protocols. See Supplementary Information for additional methods.

AFM. To determine the mechanical properties of PA hydrogels by indentation and to quantify protein tethering by force spectroscopy, a MFP-3D-Bio atomic force microscope was used. Chromium/gold-coated, silicone nitride cantilevers with pyramid-shaped tips with ~50 pN nm^{-1} nominal spring constants were used for both methods. Samples were indented at a velocity of 2 μm s^{-1} until a trigger of 2 nN was detected using. All AFM data were analysed using custom-written code in Igor Pro to determine Young's modulus as previously described[35]. PDMS substrates were indented with the same cantilevers mentioned above. In addition, a cantilever with a 45-μm-diameter polystyrene bead tip with 0.03 N m^{-1} nominal spring constant was used. For retraction experiments, samples were indented with approach and retraction velocities ranging from 1 nm s^{-1} to 10 μm s^{-1}. The substrate spring constants were determined by fitting the linear portion of the retraction curve starting at the undeformed surface.

For force spectroscopy, cantilevers were functionalized (Fig. 3a) with an anti-collagen type I antibody, or avidin using a previously established method[36,37]. Briefly, cantilevers were cleaned with chloroform and immersed in ethanolamine-HCl in dimethylsulphoxide. Tips were incubated in bis(sulphosuccinimidyl)suberate, rinsed, and then immersed either in an antibody or avidin solution to crosslink the protein to the tip. Force curves were taken in a regular 10 × 10 array of points spaced ~10 μm apart. To promote binding of the antibody to collagen or avidin to biotin, a dwell time of 1 s was added between approach and retraction cycles. Force curves were converted to force versus tip *Z*-position curves (Supplementary Fig. 6a) and then analysed for

rupture events using a previously described algorithm[38]; rupture lengths and forces were determined.

Traction force microscopy. Traction force microscopy was performed as previously described[23]. Briefly, fluorescent 0.2 μm microspheres were added to the pre-polymer solution. Substrates were functionalized and treated as described above. The microspheres underneath selected live cells were imaged with a confocal imaging system. Cells were released with trypsin and the same confocal stacks were acquired. Bead displacements were determined using a particle image velocimetry MATLAB script.

FRET. Concentrated fibronectin was denatured in guanidine hydrochloride and dual-labelled with donor and acceptor fluorophores, as previously described[13]. Denatured fibronectin was incubated with a molar excess of Alexa Fluor 546 C5 maleimide and subsequently buffer exchanged into sodium bicarbonate. The single-labelled fibronectin was then incubated with a molar excess of Alexa Fluor 488 succinimidyl ester. Unreacted donor fluorophores were removed using a spin desalting column. The emission spectrum of the dual-labelled fibronectin was characterized in varying concentrations of denaturant by fluorescence spectroscopy. The resulting emission spectrum was measured from 510 to 700 nm (Supplementary Fig. 9b) and the ratio of the maximum acceptor emission (~570 nm) to the maximum donor emission (~520 nm) was determined at each concentration of GdnHCl (Supplementary Fig. 9c). Images of the dual-labelled fibronectin were acquired using a confocal microscope and analysed using a custom MATLAB script, as previously described[14]. The mean FRET ratio within the selected regions was calculated for each cell and then averaged over all of the cells in each condition ($n = 16$ cells per condition; Fig. 2g).

See Supplementary Information for additional methods.

Received 9 January 2014; accepted 4 July 2014; published online 10 August 2014

References

1. Pelham, R. J. Jr & Wang, Y. Cell locomotion and focal adhesions are regulated by substrate flexibility. *Proc. Natl Acad. Sci. USA* **94,** 13661–13665 (1997).
2. Gilbert, P. M. *et al.* Substrate elasticity regulates skeletal muscle stem cell self-renewal in culture. *Science* **329,** 1078–1081 (2010).
3. Engler, A. J., Sen, S., Sweeney, H. L. & Discher, D. E. Matrix elasticity directs stem cell lineage specification. *Cell* **126,** 677–689 (2006).
4. Choi, Y. S., Vincent, L. G., Lee, A. R., Dobke, M. K. & Engler, A. J. Mechanical derivation of functional myotubes from adipose-derived stem cells. *Biomaterials* **33,** 2482–2491 (2012).
5. Saha, K. *et al.* Substrate modulus directs neural stem cell behavior. *Biophys. J.* **95,** 4426–4438 (2008).
6. Rowlands, A. S., George, P. A. & Cooper-White, J. J. Directing osteogenic and myogenic differentiation of MSCs: Interplay of stiffness and adhesive ligand presentation. *Am. J. Physiol. Cell Physiol.* **295,** C1037–C1044 (2008).
7. Engler, A. J., Sen, S., Sweeney, H. L. & Discher, D. E. Matrix elasticity directs stem cell lineage specification. *Cell* **126,** 677–689 (2006).
8. McBeath, R., Pirone, D. M., Nelson, C. M., Bhadriraju, K. & Chen, C. S. Cell shape, cytoskeletal tension, and RhoA regulate stem cell lineage commitment. *Dev. Cell* **6,** 483–495 (2004).
9. Dupont, S. *et al.* Role of YAP/TAZ in mechanotransduction. *Nature* **474,** 179–183 (2011).
10. Kilian, K. A., Bugarija, B., Lahn, B. T. & Mrksich, M. Geometric cues for directing the differentiation of mesenchymal stem cells. *Proc. Natl Acad. Sci. USA* **107,** 4872–4877 (2010).
11. Huebsch, N. *et al.* Harnessing traction-mediated manipulation of the cell/matrix interface to control stem-cell fate. *Nature Mater.* **9,** 518–526 (2010).
12. Khetan, S. *et al.* Degradation-mediated cellular traction directs stem cell fate in covalently crosslinked three-dimensional hydrogels. *Nature Mater.* **12,** 458–465 (2013).
13. Baneyx, G., Baugh, L. & Vogel, V. Fibronectin extension and unfolding within cell matrix fibrils controlled by cytoskeletal tension. *Proc. Natl Acad. Sci. USA* **99,** 5139–5143 (2002).
14. Smith, M. L. *et al.* Force-induced unfolding of fibronectin in the extracellular matrix of living cells. *PLoS Biol.* **5,** e268 (2007).
15. Trappmann, B. *et al.* Extracellular-matrix tethering regulates stem-cell fate. *Nature Mater.* **11,** 642–649 (2012).
16. Rossman, J. S. & Dym, C. L. *Introduction to Engineering Mechanics: A Continuum Approach* (CRC Press, 2008).
17. Plotnikov, S. V., Pasapera, A. M., Sabass, B. & Waterman, C. M. Force fluctuations within focal adhesions mediate ECM-rigidity sensing to guide directed cell migration. *Cell* **151,** 1513–1527 (2012).
18. Holle, A. W. *et al. In situ* mechanotransduction via vinculin regulates stem cell differentiation. *Stem Cells* **31,** 2467–2477 (2013).
19. Lutolf, M. P., Gilbert, P. M. & Blau, H. M. Designing materials to direct stem-cell fate. *Nature* **462,** 433–441 (2009).
20. Guilak, F. *et al.* Control of stem cell fate by physical interactions with the extracellular matrix. *Cell Stem Cell* **5,** 17–26 (2009).
21. Discher, D. E., Mooney, D. J. & Zandstra, P. W. Growth factors, matrices, and forces combine and control stem cells. *Science* **324,** 1673–1677 (2009).
22. Stellwagen, N. C. Apparent pore size of polyacrylamide gels: Comparison of gels cast and run in tris-acetate-EDTA and tris-borate-EDTA buffers. *Electrophoresis* **19,** 1542–1547 (1998).
23. Del Alamo, J. C. *et al.* Three-dimensional quantification of cellular traction forces and mechanosensing of thin substrata by fourier traction force microscopy. *PLoS ONE* **8,** e69850 (2013).
24. Ruoslahti, E. & Pierschbacher, M. D. New perspectives in cell adhesion: RGD and integrins. *Science* **238,** 491–497 (1987).
25. Engler, A. *et al.* Substrate compliance versus ligand density in cell on gel responses. *Biophys. J.* **86,** 617–628 (2004).
26. Murrell, M., Kamm, R. & Matsudaira, P. Substrate viscosity enhances correlation in epithelial sheet movement. *Biophys. J.* **101,** 297–306 (2011).
27. Bangasser, B. L., Rosenfeld, S. S. & Odde, D. J. Determinants of maximal force transmission in a motor-clutch model of cell traction in a compliant microenvironment. *Biophys. J.* **105,** 581–592 (2013).
28. Fu, J. *et al.* Mechanical regulation of cell function with geometrically modulated elastomeric substrates. *Nature Methods* **7,** 733–736 (2010).
29. Khatiwala, C. B., Peyton, S. R., Metzke, M. & Putnam, A. J. The regulation of osteogenesis by ECM rigidity in MC3T3-E1 cells requires MAPK activation. *J. Cell. Physiol.* **211,** 661–672 (2007).
30. Young, J. L. & Engler, A. J. Hydrogels with time-dependent material properties enhance cardiomyocyte differentiation *in vitro*. *Biomaterials* **32,** 1002–1009 (2011).
31. Chopra, A. *et al.* Reprogramming cardiomyocyte mechanosensing by crosstalk between integrins and hyaluronic acid receptors. *J. Biomech.* **45,** 824–831 (2012).
32. Kong, H. J., Polte, T. R., Alsberg, E. & Mooney, D. J. FRET measurements of cell-traction forces and nano-scale clustering of adhesion ligands varied by substrate stiffness. *Proc. Natl Acad. Sci. USA* **102,** 4300–4305 (2005).
33. Choi, Y. S. *et al.* The alignment and fusion assembly of adipose-derived stem cells on mechanically patterned matrices. *Biomaterials* **33,** 6943–6951 (2012).
34. Carpenter, A. E. *et al.* CellProfiler: Image analysis software for identifying and quantifying cell phenotypes. *Genome Biol.* **7,** R100 (2006).
35. Kaushik, G. *et al.* Measuring passive myocardial stiffness in *Drosophila melanogaster* to investigate diastolic dysfunction. *J. Cell. Mol. Med.* **16,** 1656–1662 (2012).
36. Bonanni, B. *et al.* Single molecule recognition between cytochrome C 551 and gold-immobilized azurin by force spectroscopy. *Biophys. J.* **89,** 2783–2791 (2005).
37. Chirasatitsin, S. & Engler, A. J. Detecting cell-adhesive sites in extracellular matrix using force spectroscopy mapping. *J. Phys. Condens. Matter* **22,** 194102 (2010).
38. Fuhrmann, A., Anselmetti, D., Ros, R., Getfert, S. & Reimann, P. Refined procedure of evaluating experimental single-molecule force spectroscopy data. *Phys. Rev. E* **77,** 031912 (2008).

Acknowledgements

The authors thank M. Joens, J. Kasuboski and J. Fitzpatrick at the Waitt Advanced Biophotonics Center at the Salk Institute (supported by NCI P30 Cancer Center Support Grant CA014195-40 and NINDS P30 Neuroscience Center Core Grant NS072031-03A1 and by the W. M. Keck Foundation) for technical assistance with microscopy, and W. Murphy (University of Wisconsin), T. McDevitt (Georgia Tech) and J. C. del Alamo (UC San Diego) for helpful conversations. The National Institutes of Health (DP02OD006460 to A.J.E.), the Human Frontiers Science Program (RGY0064/2010 to A.J.E.), the National Science Foundation Graduate Research Fellowship Program (to J.H.W., L.G.V. and H.T-W.), the Siebel Scholars Program, and the Achievement Rewards for College Scientists (to L.G.V.) supported this work.

Author contributions

All authors contributed to the design of experiments. Y.S.C., K.C.H. and S.C. characterized the hydrogel substrates. H.T-W. characterized and performed experiments with the FRET probe. J.H.W., L.G.V. and A.F. conducted all other experiments and performed the data analysis. J.H.W., L.G.V. and A.J.E. wrote the manuscript.

Additional information

Supplementary information is available in the online version of the paper. Reprints and permissions information is available online at www.nature.com/reprints. Correspondence and requests for materials should be addressed to A.J.E.

Competing financial interests

The authors declare no competing financial interests.